HIGGS PRODUCTION AT NNLOPS

E. RE
Rudolf Peierls Centre for Theoretical Physics, Department of Physics, University of Oxford, Oxford, OX1 3NP, United Kingdom

We describe the method used to build a simulation of Higgs boson production accurate at next-to-next-to-leading order and matched to a parton shower. The adopted procedure makes use of a combination of the POWHEG and MiNLO methods. We also use results from HNNLO as final input to reach the claimed accuracy. Results for typical observables are shown.

1 Introduction

During the last decade a major research effort in the Monte Carlo community has been devoted to the development of NLOPS tools, *i.e.* tools that allow a matching of next-to-leading order (NLO) computations with parton showers (PS), thereby bringing NLO accuracy into standard Monte Carlo event generators [1]. Among many proposals, there are currently two well-established NLOPS approaches, namely POWHEG [2,3] and MC@NLO [4], which have now become the methods of choice used by experimental collaborations in many analyses being carried out at the LHC.

Despite in general NLO accuracy is enough for the majority of processes studied at the LHC, it is known that for some of them the inclusion of next-to-next-to-leading order (NNLO) effects is necessary: this is the case when the experimental accuracy demands $\mathcal{O}(1\%)$ precision in theoretical predictions, or when NNLO effects are large. Paramount examples of these 2 situations are Drell-Yan and (gluon-fusion-initiated) Higgs production, respectively. In these cases, it is clearly desirable to include NNLO corrections into Monte Carlo programs, if one wants to have a simulation tool which is flexible and accurate enough at the same time.

A NNLOPS simulation was achieved recently for Higgs production [5]. In this document the theoretical ingredients (namely the POWHEG and MiNLO approaches) underlying this result are quickly summarised, the method used to combine them is outlined, and selected results are shown.

2 Higgs production at NNLOPS

2.1 POWHEG

The POWHEG method is a prescription to match NLO calculations with parton shower generators avoiding double counting of real emissions and virtual corrections. In the POWHEG formalism, the generation of the hardest emission is performed first, according to the distribution given by

$$d\sigma = \bar{B}\left(\Phi_B\right)\, d\Phi_B \left[\Delta_R\left(p_T^{\min}\right) + \frac{R\left(\Phi_R\right)}{B\left(\Phi_B\right)}\,\Delta_R\left(k_T\left(\Phi_R\right)\right)\, d\Phi_{\rm rad}\right], \tag{1}$$

where $B(\Phi_B)$ is the leading order term,

$$\bar{B}(\Phi_B) = B(\Phi_B) + \left[V(\Phi_B) + \int d\Phi_{\rm rad}\, R(\Phi_R) \right] \tag{2}$$

is the NLO differential cross section integrated on the radiation variables while keeping the Born kinematics fixed ($V(\Phi_B)$ and $R(\Phi_R)$ stand respectively for the virtual and the real corrections), and $\Delta_R(p_T) = \exp\left[-\int d\Phi_{\rm rad} \frac{R(\Phi_R)}{B(\Phi_B)} \theta(k_T(\Phi_R) - p_T) \right]$ is the POWHEG Sudakov form factor. With $k_T(\Phi_R)$ we denote the transverse momentum of the emitted particle off a Born-like kinematics Φ_B. It can be shown that by showering the partonic events generated according to eq. (1), one obtains NLOPS-accurate results, *i.e.* Sudakov suppression close to the soft-collinear regions, LO accuracy in the regions where the POWHEG emission is widely-separated from the other coloured particles in Φ_B, and, crucially, NLO accuracy for inclusive observables.

From the NLOPS-matching point of view, the more challenging processes currently described with this approach are $2 \to 3$ and $2 \to 4$ processes, with at most 2 light jets at LO [6,7,8,9,10]. One should notice that when one or more jets are present at LO (as in the $H+1$ jet case), the $\bar{B}$ function needs to be regulated from the divergences arising when jets in the LO kinematics become unresolved [11]: as a consequence, a POWHEG simulation of $H+1$ jet cannot be used to describe Higgs production observables that are fully inclusive over QCD radiation.

2.2 MiNLO

The MiNLO procedure [12] was originally introduced as a prescription to a-priori choose the renormalisation (μ_R) and factorisation (μ_F) scales in multileg NLO computations: since these computations can probe kinematical regimes involving several different scales, the choice of μ_R and μ_F is indeed ambiguous, and the MiNLO method addresses this issue by consistently including CKKW-like corrections [13,14] into a standard NLO computation. By clustering with a k_T-measure the momenta of each phase-space point sampled, one can define the "most-probable" branching history that would have produced such a kinematics: similarly to what is done in parton showers, the argument of each power of $\alpha_{\rm S}$ is then found from the transverse momentum of the splitting occurring at each nodal point of the skeleton built from clustering, and a prescription for μ_F is given as well. The result is also corrected by means of Sudakov form factors (called MiNLO-Sudakov FF's in the following) associated to internal lines, accounting for the large logarithms that arise when the clustered event contains well separated scales.

Because of the presence of MiNLO-Sudakov FF's associated to the Born-like kinematics, the integration over the full phase space Φ_B can be performed without generation cuts, yielding finite results also when jets in the LO kinematics become unresolved. As a consequence, the MiNLO procedure can be used within the POWHEG formalism to regulate the $\bar{B}$ function for processes involving jets at LO [12,15,16,17], without using external cuts or variants thereof. In particular, in the $H+1$ jet case, the master formula for generating the hardest emission contains the following MiNLO-improved $\bar{B}$ function

$$\begin{aligned} \bar{B}_{\texttt{HJ-MiNLO}} &= \alpha_{\rm S}^2(M_H)\alpha_{\rm S}(q_T)\Delta_g^2(q_T, M_H) \\ &\times \left[B(1 - 2\Delta_g^{(1)}(q_T, M_H)) + \alpha_{\rm S} V(\bar{\mu}_R) + \alpha_{\rm S} \int d\Phi_{\rm rad} R \right], \end{aligned} \tag{3}$$

to be contrasted with the normal POWHEG $\bar{B}$ function, that would read for this process

$$\bar{B}_{\texttt{HJ}} = \alpha_{\rm S}^3(\mu_R)\left[B + \alpha_{\rm S} V(\mu_R) + \alpha_{\rm S} \int d\Phi_{\rm rad} R \right]. \tag{4}$$

In eq. (3) q_T and M_H are the Higgs transverse momentum and virtuality, $\bar{\mu}_R$ is set to $(M_H^2 q_T)^{1/3}$ in accordance with the MiNLO prescription and $\Delta_g(q_T, Q) = \exp\left\{ -\int_{q_T^2}^{Q^2} \frac{dq^2}{q^2} \frac{\alpha_{\rm S}(q^2)}{2\pi} \left[A_g \log \frac{Q^2}{q^2} + \right.\right.$

$B_g\Big]\Big\}$ is the MiNLO-Sudakov FF associated to the jet present at LO. The term in brackets multiplying B contains $\Delta_g^{(1)}(q_T, Q)$, that is the $\mathcal{O}(\alpha_s)$ expansion of Δ_g.

In ref. [15] it was found that not only eq. (3) allows to integrate over the full phase space associated with the "LO" jet, but also that, with relatively minor improvements, the result so-obtained is formally NLO accurate also for fully-inclusive observables.

2.3 NNLOPS

The $H+1$ jet POWHEG implementation enhanced with the improved MiNLO procedure previously outlined can be used to reach NNLOPS accuracy. In fact, since such a simulation gives a NLO-accurate prediction of the Higgs rapidity (y), then the function $W(y)$, defined as

$$W(y) = \frac{(d\sigma/dy)_{\text{NNLO}}}{(d\sigma/dy)_{\texttt{HJ-MiNLO}}}\,, \tag{5}$$

can be used to reweight each HJ-MiNLO-generated event, thereby obtaining a NNLOPS simulation of inclusive Higgs production. By NNLOPS we mean a fully-exclusive Monte Carlo simulation of Higgs-production which is NNLO accurate for fully-inclusive observables, as well as LO (NLO) accurate for $H+2(1)$ jet observables [15,5]. Since we are reweighting the events with $W(y)$, the Higgs rapidity is NNLO accurate by construction, whereas the NLO accuracy of the 1-jet region, inherited from the underlying HJ-MiNLO simulation, is not spoilt, because the first non-controlled terms in the whole simulation are $\mathcal{O}(\alpha_s^5)$: this follows from the fact that $W(y) = 1 + \mathcal{O}(\alpha_s^2)$, as can be seen expanding numerator and denominator in eq. (5).

In ref. [5] the following generalisation of eq. (5) was used:

$$W(y, p_T) = h(p_T)\frac{\int d\sigma_{\text{NNLO}}\delta(y - y(\Phi)) - \int d\sigma^B_{\texttt{HJ-MiNLO}}\delta(y - y(\Phi))}{\int d\sigma^A_{\texttt{HJ-MiNLO}}\delta(y - y(\Phi))} + (1 - h(p_T))\,, \tag{6}$$

where we have split the HJ-MiNLO differential cross section among $d\sigma^A = d\sigma\ h(p_T)$ and $d\sigma^B = d\sigma\ (1 - h(p_T))$, with $h(p_T) = \frac{(\beta m_H)^2}{(\beta m_H)^2 + p_T^2}$. The profiling function h controls where the NLO-to-NNLO correction is spread: as 2nd argument of W the transverse momentum of the leading jet was used, and we have chosen $\beta = 1/2$, which implies that the NNLO correcting factor W is effectively applied in the region $p_T \lesssim m_H/2$.

2.4 Results

In our simulation, the central value for $d\sigma_{\text{NNLO}}$ was obtained with HNNLO [18,19], setting $\mu_R = \mu_F = m_H/2$. We refer to ref. [5] for details on how scales were varied to obtain uncertainty bands.

A comparison between our NNLOPS simulation and HNNLO is shown in fig. 1 (partonic events were showered with PYTHIA 6 [20]): as expected, the NNLOPS simulation reproduces extremely well the NNLO results for the Higgs rapidity both in the central value and in the uncertainty band obtained by scale variation.

Fig. 2 shows the Higgs transverse momentum p_T^H. We compare our simulation with HQT [21,22], whose central value is obtained with $Q_{\text{res}} = m_H/2$ and $\mu_R = \mu_F = m_H/2$. The HQT result corresponds to a NNLL prediction for p_T^H, matched to the fully inclusive cross section at NNLO. Here we notice that the two results are almost completely contained within each other's uncertainty band in the region of low-to-moderate transverse momenta. The central values at small momenta also exhibit a very good agreement, supporting our choice for β. The difference in the large-p_T tail is not a reason of concern, and it is expected since the two predictions use different scales at large p_T, as explained in ref. [5].

Finally, we also mention that a comparison among NNLOPS and NNLL+NNLO predictions from JETVHETO [23] was successfully carried out for the jet veto efficiency, defined as the cross

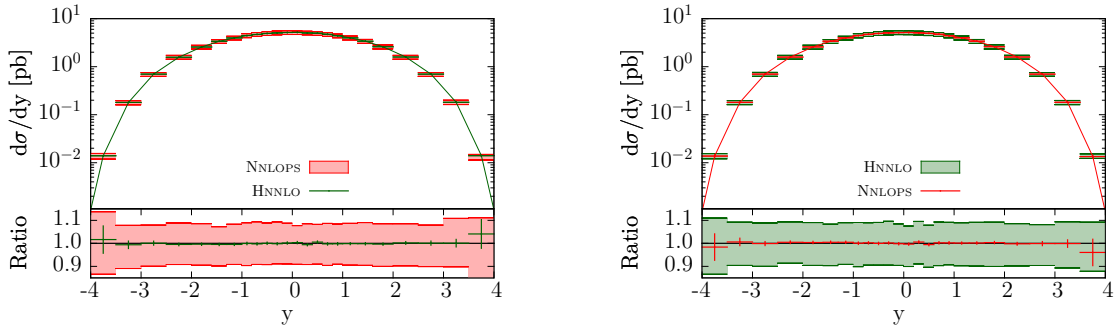

Figure 1 – Comparison of the NNLOPS (red) and HNNLO (green) results for the Higgs fully inclusive rapidity distribution. On the left (right) plot only the NNLOPS (HNNLO) uncertainty is displayed. The lower left (right) panel shows the ratio with respect to the NNLOPS (HNNLO) prediction obtained with its central scale choice.

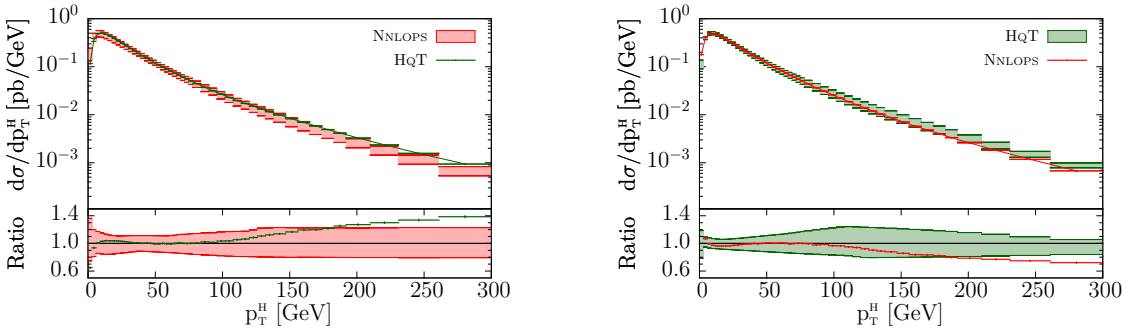

Figure 2 – Comparison of the NNLOPS (red) with the NNLL+NNLO prediction of HQT (green) for the Higgs transverse momentum. In HQT we keep the resummation scale $Q_{\rm res}$ always fixed to $m_H/2$ and vary μ_R and μ_F. On the left (right), the NNLOPS (HQT) uncertainty band is shown. In the lower panel, the ratio to the NNLOPS (HQT) central prediction is displayed.

section for producing the Higgs boson and no jets with transverse momentum greater than a given value ($p_{\rm T,veto}$), divided by the respective total inclusive cross section. The central predictions of the two programs are never out of agreement by more than 5-6%, and the two sets of predictions lie within each other's error bands essentially everywhere over all values of $p_{\rm T,veto}$, as shown in ref. [5].

Acknowledgments

NNLOPS results presented here have been obtained in ref. [5], in collaboration with K. Hamilton, P. Nason and G. Zanderighi. The original proposal of reaching NNLOPS accuracy from MiNLO-merged NLOPS simulations was outlined in ref. [15], which was co-authored by C. Oleari. The author acknowledges the organising committee for the financial help received to cover the living expenses.

References

1. A. Buckley, J. Butterworth, S. Gieseke, D. Grellscheid, S. Hoche, H. Hoeth, F. Krauss and L. Lonnblad *et al.*, Phys. Rept. **504**, 145 (2011) [arXiv:1101.2599 [hep-ph]].
2. P. Nason, JHEP **0411**, 040 (2004) [hep-ph/0409146].
3. S. Frixione, P. Nason and C. Oleari, JHEP **0711**, 070 (2007) [arXiv:0709.2092 [hep-ph]].
4. S. Frixione and B. R. Webber, JHEP **0206**, 029 (2002) [hep-ph/0204244].
5. K. Hamilton, P. Nason, E. Re and G. Zanderighi, JHEP **1310**, 222 (2013) [arXiv:1309.0017 [hep-ph]].
6. J. M. Campbell, R. K. Ellis, R. Frederix, P. Nason, C. Oleari and C. Williams, JHEP

1207, 092 (2012) [arXiv:1202.5475 [hep-ph]].
7. E. Re, JHEP **1210**, 031 (2012) [arXiv:1204.5433 [hep-ph]].
8. B. Jager, S. Schneider and G. Zanderighi, JHEP **1209**, 083 (2012) [arXiv:1207.2626 [hep-ph]].
9. B. Jager and G. Zanderighi, JHEP **1304**, 024 (2013) [arXiv:1301.1695 [hep-ph]].
10. B. Jager, A. Karlberg and G. Zanderighi, JHEP **1403**, 141 (2014) [arXiv:1312.3252 [hep-ph]].
11. S. Alioli, P. Nason, C. Oleari and E. Re, JHEP **1101**, 095 (2011) [arXiv:1009.5594 [hep-ph]].
12. K. Hamilton, P. Nason and G. Zanderighi, JHEP **1210**, 155 (2012) [arXiv:1206.3572 [hep-ph]].
13. S. Catani, F. Krauss, R. Kuhn and B. R. Webber, JHEP **0111**, 063 (2001) [hep-ph/0109231].
14. L. Lonnblad, JHEP **0205**, 046 (2002) [hep-ph/0112284].
15. K. Hamilton, P. Nason, C. Oleari and G. Zanderighi, JHEP **1305**, 082 (2013) [arXiv:1212.4504].
16. J. M. Campbell, R. K. Ellis, P. Nason and G. Zanderighi, JHEP **1308**, 005 (2013) [arXiv:1303.5447 [hep-ph]].
17. G. Luisoni, P. Nason, C. Oleari and F. Tramontano, JHEP **1310**, 083 (2013) [arXiv:1306.2542 [hep-ph]].
18. S. Catani and M. Grazzini, Phys. Rev. Lett. **98**, 222002 (2007) [hep-ph/0703012].
19. M. Grazzini, JHEP **0802**, 043 (2008) [arXiv:0801.3232 [hep-ph]].
20. T. Sjostrand, S. Mrenna and P. Z. Skands, JHEP **0605**, 026 (2006) [hep-ph/0603175].
21. G. Bozzi, S. Catani, D. de Florian and M. Grazzini, Nucl. Phys. B **737**, 73 (2006) [hep-ph/0508068].
22. D. de Florian, G. Ferrera, M. Grazzini and D. Tommasini, JHEP **1111**, 064 (2011) [arXiv:1109.2109 [hep-ph]].
23. A. Banfi, P. F. Monni, G. P. Salam and G. Zanderighi, Phys. Rev. Lett. **109**, 202001 (2012) [arXiv:1206.4998 [hep-ph]].